frontiers in Built Environment

ORIGINAL RESEARCH
published: 28 July 2021
doi: 10.3389/fbuil.2021.673346

# The Effect of the Addition of Graphene Nanoplatelets on the Selected Properties of Cementitious Composites

*Zhi Ge[1], Jin Qin[1], Renjuan Sun[1], Yanhua Guan[1], Hongzhi Zhang[1,2]* and Zheng Wang[3]*

[1]School of Qilu Transportation, Shandong University, Jinan, China, [2]Suzhou Research Institute, Shandong University, Suzhou, China, [3]Shandong Hi-Speed Group, Jinan, China

The aim of the current study is to investigate the properties of graphene nanoplatelets-cementitious composites in a consistent sense. The influence of the addition of 2D graphene nanoplatelets (GNPs) on the workability, setting time, flowability, strengths and piezoresistive properties were studied. The dosage of the GNPs is 0 0.05, 0.1, 0.3, 0.5, 0.7, and 1.0 wt% of the binder material. PVP type surfactant was used to disperse GNPs. The experimental results showed that the addition of GNPs increases the water requirement for normal consistency and decreases the flowability. A small amount of GNPs (0.05 wt%) can facilitate the setting. When the dosage of GNPs is above 0.1 wt%, it leads to the delay of the setting time. In terms of the strengths, the addition of GNPs can considerably promote the flexural strength, while the compressive strength is slightly decreased until 28 days. A pre-treatment procedure consisting of drying specimens at 105°C for 1 day can be regarded as a proper way to enhance the piezoresistive properties of the GNPs-mortar. Piezoresistive properties under two different cyclical loading schemes were measured using the GNPs-mortar with 1 wt% GNPs. It has been shown that the average resistance change rate increases with the amplitude increasing and a reduction is observed for the sustained cyclical loading condition. In the end, the influence of the microcracks on the piezoresistive properties was investigated. This study will contribute to future developments of cementitious composites incorporating GNPs for a variety of applications.

**Keywords: graphene nanoplatelets, cement composites, fresh properties, mechanical properties, piezoresistive properties**

OPEN ACCESS

***Edited by:***
*Biranchi Panda,*
*Indian Institute of Technology Guwahati, India*

***Reviewed by:***
*Suvash Chandra Paul,*
*International University of Business Agriculture and Technology, Bangladesh*
*Tanvir Qureshi,*
*University of the West of England, United Kingdom*

****Correspondence:***
*Hongzhi Zhang*
*hzzhang@sdu.edu.cn*

***Specialty section:***
*This article was submitted to Sustainable Design and Construction, a section of the journal Frontiers in Built Environment*

***Received:*** *27 February 2021*
***Accepted:*** *07 June 2021*
***Published:*** *28 July 2021*

***Citation:***
*Ge Z, Qin J, Sun R, Guan Y, Zhang H and Wang Z (2021) The Effect of the Addition of Graphene Nanoplatelets on the Selected Properties of Cementitious Composites. Front. Built Environ. 7:673346. doi: 10.3389/fbuil.2021.673346*

## INTRODUCTION

Concrete structures face dynamic loading from different sources, such as high-speed wind and earthquakes. The dynamic loads may cause severe vibrations and large deflections, resulting in cracks in the concrete. The cracks not only threat the safety of the structures, but also bring discomfort to the residents. In order to reduce failure risk or maintenance costs, the real-time monitoring and evaluation of concrete structures have generated considerable research efforts. The conventional approaches include using strain gages, optical fibers, and piezoelectric sensors (Li et al., 2001; Zhang et al., 2002; Luo et al., 2013). However, it has been reported that these methods exhibit durability issues and require expensive external facilities (Chen and Chung, 1996). On the other hand,

development of piezoresistive cement-based materials have shed much light on the transformation sensing technology applicable to concrete structures (Shi and Chung, 1999; Liu et al., 2018; Yoo et al., 2018).

The use of graphene nanoplatelets (GNPs) has been reported to increase the electrical conductivity of cementitious composites (Le et al., 2014). A comprehensive review of incorporating GNPs into cement paste has been conducted (Du et al., 2020; Lin and Du, 2020). GNPs are a type of two-dimensional material. They are made up of several layers of graphene sheets with a thickness in the range of 3–100 nm (Chu et al., 2013). To improve the dispersion efficiency, a wide range of dispersion methods have been employed, mostly using sonication (Qureshi and Panesar, 2019) [usually in combination with surface modification of the nanomaterial either chemically (Qureshi et al., 2019; Qureshi and Panesar, 2020) or physically, *via* the addition of a surfactant to the nanomaterial dispersion (Wei et al., 2011; Pu et al., 2012; Gholampour et al., 2017; Birenboim et al., 2019)]. Compared with single layer graphene, GNPs have the advantage of having great electrical conductivity (Xu and Zhang, 2017; Jaitanong et al., 2018; Dong et al., 2019), reinforcing their function due to their monolayer structure and low-cost (Sun et al., 2017). It has been reported that an addition of 0.05 wt% GNPs leads to an increase of both flexural and compressive strength by around 20 and 5% respectively (Wang et al., 2016). Similar results have been reported in other studies (Alkhateb et al., 2013; Liu et al., 2016). Toughness can also be improved by using modified GNPs (Wang and Pang, 2019). However, different results were obtained by Wang and Shuang (2018) due to the different dispersion and mixing procedures and mixing proportions. Micromechanical models have been developed by Li et al. (2020) to predict the relaxation moduli of the composites. Regarding the durability properties, it has been shown that the addition of 2.5 wt% GNPs of the binder leads to a considerable growth in the water and chloride penetration resistances (Du and Pang, 2015). Furthermore, the freeze/thaw resistance and corrosion resistance are improved as well by various dosages of GNPs (Tong et al., 2016; Chen et al., 2019).

Prior to GNPs' application, a comprehensive study is required. However, little research reports the fresh properties, hardened strengths, and piezoresistive properties for a unique mixture. As the used GNPs type, dosage, binder material, as well as dispersion and mixing procedure all have significant influence on the performances of the GNPs' cement composites, it is difficult to have a thorough understanding of such materials.

To this end, the effect of GNPs addition (i.e., 0, 0.05, 0.1, 0.3, 0.5, 0.7, and 1 wt% by the binder weight) on the fresh properties, hardened mechanical properties, and piezoresistive properties is studied in a consistent sense. The influence of the GNPs addition on the workability, setting time, and flowability were investigated first. Afterwards, the development of the flexural strength and compressive strength were studied. The piezoresistive properties of the GNPs-mortar were measured using a four-probe system under cyclic compressive loads. The average resistance change rate was used to represent the piezoresistive properties of specimens under different loading conditions. The underlined mechanisms for experimental observations were discussed. The findings of this study provide insights into properties of GNPs cement composites in a consistent way and reveal their practical implications.

# MATERIALS AND METHODS

## Materials

Ordinary Portland cement 42.5 and Class F fly ash were used as binder materials in the current study. Chemical composition of the used cement is shown in **Supplementary Table S1**. C-500 graphene nanoplatelets (GNPs) purchased from XG science were used. **Supplementary Tables S2, S3** list its mechanical properties. A polyvinyl pyrrolidone (PVP) type dispersant supplied by Sinopharm Chemical Reagent Co., Ltd with a relatively stable dispersing performance in alkaline solution and salt solution was selected. It has a molecular formula of $(C_6H_9NO)_n$. Its technical index is present in **Supplementary Table S4**. Quartz sand with a fineness range in between 124 and 178 μm was used. The workability was adjusted by the polycarboxylate superplasticizer. The hypromellose with a viscosity grade of 150 was used as thickener to modify the viscosity of fresh mortar mixture.

## Mix Proportion Design and Sample Preparation

One control mix with no GNP and six batches of the GNP dosages (0.05, 0.1, 0.3, 0.5, 0.7, and 1.0 wt% of the binder material) were prepared as presented in **Table 1** to study the influence of GNP dosage on the properties of cementitious composites. GNP was dispersed in water prior to mixing with binder materials. The PVP type dispersant was mixed with deionized water with a dosage of 10 mg/ml to improve the dispersion effectiveness. High speed shearing dispersion was conducted for 15 min. This was followed by another 15 min dispersion using probe ultrasonic with a speed of 4,000 r/min. After the dispersion, no visible solid residue was observed at the bottom.

A JJ-5 mixer was then used for the mixing. The fly ash and cement paste were first mixed with a low speed for 2 min. Afterwards, the water and GNP solution was added followed by another 2 min mixing with a high speed. The mix was then used for the following test.

## Testing Methods

### Workability and Setting Time

Blended cement and fly ash paste (with the same mass ratio to **Table 1**) having various xGNP-C-500 dosages (0, 0.05, 0.1, 0.3, 0.5, 0.7 w%, and wt% of the binder materials) were prepared for the workability measurements. The water requirement for normal consistency approach was used. It was conducted following China National Standard GB/T 1346-2011 (test methods for water requirement of normal consistency, setting time, and soundness of the Portland cement) using Vicat apparatus. The Vicat proof bar has a mass of 300 ± 1 g and a diameter of 10 ± 0.05 mm. In the test, the normal consistency is defined as the status of the paste that the Vicat proof bar sinks

**TABLE 1 |** Mix proportion of mortar fluidity test.

| Mix | xGNP-C-500 (wt% of cement) | Cement (kg/m³) | Fly ash (kg/m³) | Quartz sand (kg/m³) | B/c | Thickener (kg/m³) | Superplastersizer (kg/m³) |
|---|---|---|---|---|---|---|---|
| Control | 0 | 570 | 684 | 455 | 0.264 | 0.57 | 2 |
| GNPs-005 | 0.05 | 570 | 684 | 455 | 0.264 | 0.57 | 2 |
| GNPs-010 | 0.1 | 570 | 684 | 455 | 0.264 | 0.57 | 2 |
| GNPs-030 | 0.3 | 570 | 684 | 455 | 0.264 | 0.57 | 2 |
| GNPs-050 | 0.5 | 570 | 684 | 455 | 0.264 | 0.57 | 2 |
| GNPs-070 | 0.7 | 570 | 684 | 455 | 0.264 | 0.57 | 2 |
| GNP-100 | 1 | 570 | 684 | 455 | 0.264 | 0.57 | 2 |

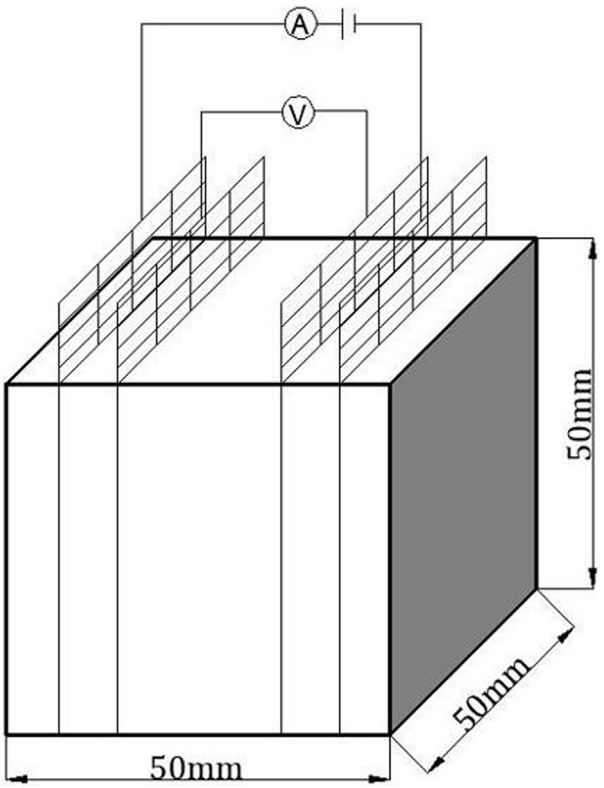


**FIGURE 1 |** Schematic diagram of electrical resistance measurement by four-probe method.

into the paste with a distance to the bottom of 6 ± 1 mm. The w/b ratio which meets this criterion is determined as the water requirement of normal consistency.

The setting time test consists of initial setting and final setting time determination using Vicat apparatus. It was conducted following the Standard GB/T 1346. A Vicat needle with a diameter of 1.13 ± 0.05 mm was used for the measurements.

## Flowability

Flowability of all the mixes was measured through mini slump tests as specified in the China National Standard GB/T 2419-2016 (test method for fluidity of cement mortar). The used cone mold has a bottom diameter of 60 mm, top diameter of 36 mm, and height of 60 mm.

## Mechanical Properties

The flexural and compressive strengths were measured according to China National Standard GB/T 17,671-1999 "Testing method for strength of cement mortar". For the test, prisms with a size of 40 mm × 40 mm × 160 mm were used. After casting, the specimens were cured for 24 h under sealed conditions with a temperature of 20 ± 1°C. Subsequently, the samples were demolded and cured in a standard curing room with a temperature of 20 ± 1°C and a relative humidity of 98 ± 2 until the test. The strengths were measured at 3, 7, and 28 days. Three specimens were tested for each condition. The prism was first used for flexural strength determination through a three-point bending test. This was followed by a uniaxial compression test performed on halves of the prisms for the compressive strength determination.

## Piezoresistive Properties

The piezoresistive properties of the GNPs-mortar specimens were measured by the four-probe method, see **Figure 1**. This method is more stable compared with the two-probe method (Han and Ou, 2007), as it avoids the possible influence of the contact resistance between the probes and cement composites compared. During the measurement, 305CF DC power was used. Voltage and current were monitored by digital multimeter supplied by Keithley Instruments. For the test, 28 days' cured cubic specimens with size lengths of 5 cm were used.

Water within the capillary pores can significantly influence the piezoelectric properties (Tao et al., 2019). Therefore, drying is required prior to the piezoelectric measurements. To determine an optimized approach for drying, two pre-treatment (drying) conditions were conducted before the measurements. They are: 1) drying at 40°C for 14 days and 2) drying at 105°C for 1 day.

After drying, an initial resistance was measured. Note that specimens were painted for the insulation, see **Figure 2A**. The specimen was then loaded under uniaxial compression by a universal testing machine, see **Figure 2B**. A cyclical load, i.e., 10–40 kN (4–16 MPa), with cycles was used for the loading process. Data from the last five cycles were used to calculate the average resistance change rate for each condition.

The optimized mix (GNPs-100) and drying approach (105°C for 1 day) was then used to measure the Piezoresistive properties under cyclical loading. The two following loading schemes were used. The first consists of a triangular wave having eight load amplitudes 10–80 kN (4–32 MPa) with a stepwise increase of

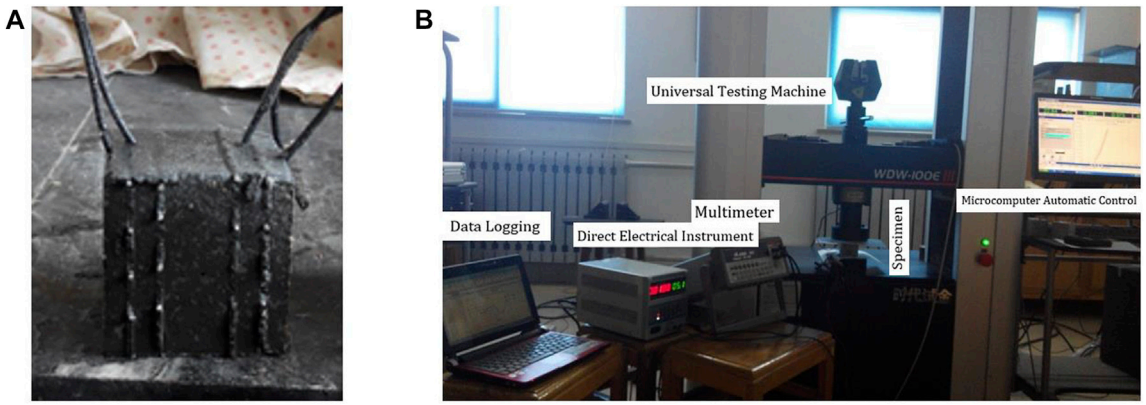


**FIGURE 2 | (A)** Cement-based composites with GNP specimen for electrical resistance test; **(B)** Electrical resistance test on site.

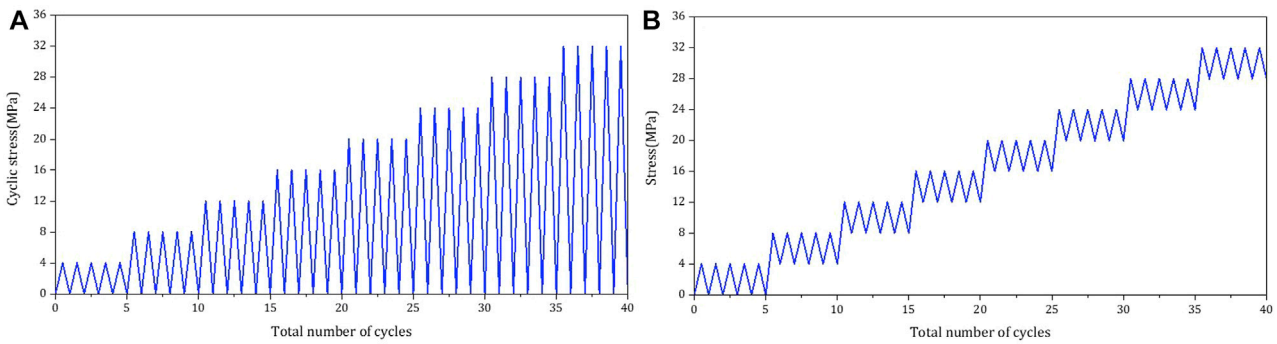


**FIGURE 3 |** Loading method: **(A)** free cycle and **(B)** load cycle.

10 kN (4 MPa), see **Figure 3A**. The second loading protocol was shown in **Figure3B**. It consists of eight load levels with the same amplitude (4 MPa) with an increase of 10 kN (4 MPa). The first loading scheme reflects the piezoresistive properties of GNPs-mortar specimens without pre-loading while the second studies the influence of pre-load stress level on the piezoresistive properties.

To investigate the influence of microcracks on the piezoresistive properties, the GNPs-100 specimens (dried 105°C for 1 day) were loaded by a cyclic load with 10 loading cycles prior to the piezoresistive properties measurements. The minimal and maximum loads are 32 and 36 MPa, respectively. It is expected that this pre-loading procedure would generate microcracks inside the investigated materials (Zhang et al., 2020; Hou et al., 2021). The piezoresistive properties measurements were then carried out under the aforementioned two cyclical loading conditions.

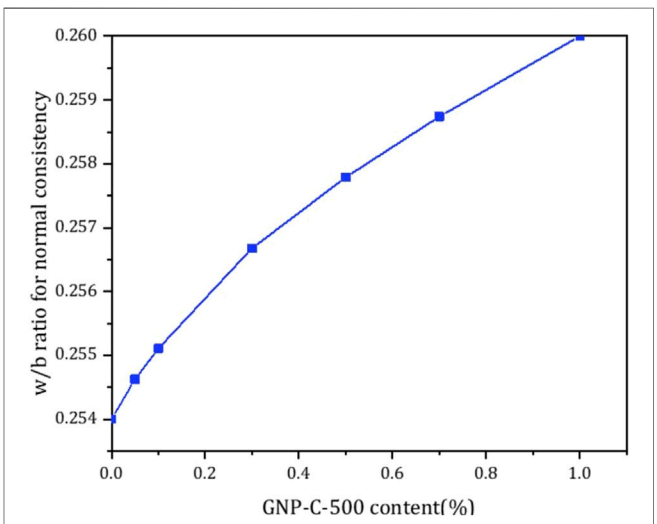


**FIGURE 4 |** The effects of GNP-C-500 content on w/b ratio for normal consistency.

# RESULTS AND DISCUSSION

## Physical Properties

### Workability and Setting Time

**Figure 4** shows the influence of GNP-C-500 content on the water requirement for normal consistency. GNP-C-500 has a negative effect on the workability of the paste. With the dosage of GNP-C-500 increasing from 0 to 1 wt%, the w/c ratio required for the normal consistency rises up from 0.254 to 0.260. It should be

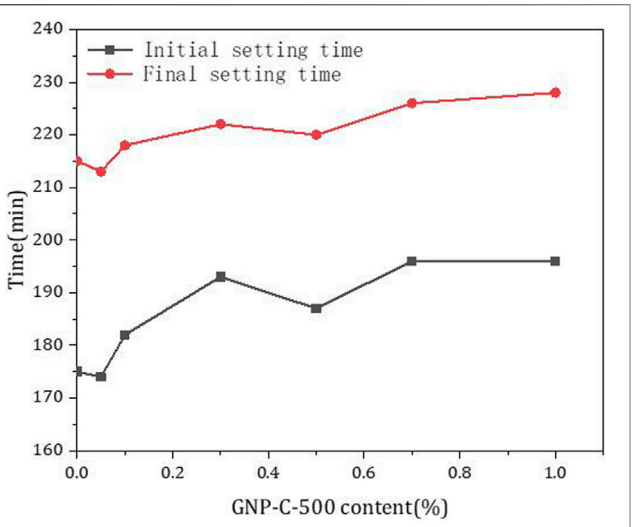


**FIGURE 5 |** The effects of GNP-C-500 content on setting time.

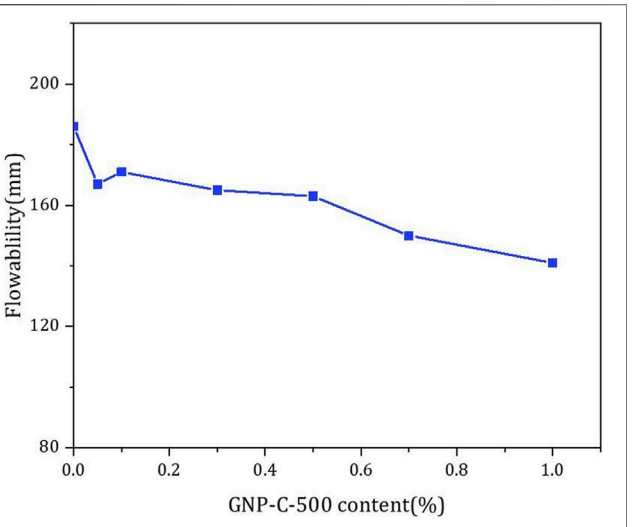


**FIGURE 6 |** The effects of GNP-C-500 content on flowability.

noted that the w/b ratio increasing rate is reduced with the GNP-C-500 dosage increasing.

The initial setting time and final setting time of the mixes having a normal consistency are presented in **Figure 5**. In general, both the final setting time and initial setting time increases with the GNP-C-500 dosage. When 1 wt% GNP-C-500 was used, the initial setting time and final setting time were delayed by 34 and 45 min respectively. However, a small drop of setting time was observed when 0.05 wt% GNP-C-500 was used. GNPs may play a role in nucleation sites (Peyvandi et al., 2013). When the content is above 0.1 wt%, the GNP-C-500 slows the setting of the blended paste. This can be attributed to the agglomeration of GNPs, which reduces the hydration rate of cement paste (Baomin and Shuang, 2019).

### Flowability of Cement Mortar

Flowability measurement results are shown in **Figure 6**. It can be seen that the flowability is significantly influenced by the addition of GNP. In general, the addition of GNP leads to a reduction of the flowability. When a GNP dosage of 1 wt% is used, the spread diameter decreases to 140 mm, by 25% lower than the control mix. A similar trend has been reported in other studies (Du and Pang, 2018). A possible reason for the reduction in slump value can be associated with the flocculation phenomena caused by the high aspect ratio and strong van der Waals forces of GNPs. More specifically, GNPs are dispersed in the fresh mortar in the form of aggregate, which hinders the normal flow of the fresh mortar. This can be avoided by modifying the GNPs using silane coupling agent (Guo et al., 2020).

### Mechanical Properties of Cement Mortar

The measured flexural and compressive strengths are shown in **Figure 7**. At 3 days, the flexural strength has a significant increase when the addition of GNP-C-500 is no more than 0.1 wt%. Once the dosage exceeds this value, no significant changes in flexural strength is observed. On the other hand, the compressive remains almost unchanged. In terms of the specimens cured for 7 days, a contrary trend is observed for the flexural and compressive strengths. Specifically, the compressive strength decreases with the GNP-C-500 dosage and the reduction rate decreases gradually. While, with the GNP-C-500 dosage increasing, the flexural strength grows more significantly. However, it is worth noting that the GNPs-005 has a compressive strength higher than bulk paste while the tensile strength is lower. When it comes to 28 days, a significant increase of compressive strength is observed when 0.05 wt% GNP-C-500 was added. This is followed by a slight decline with GNP-C-500 increasing. The slight reduction can be caused by the poor dispersion when a high dosage of GNP is used. Furthermore, there is a growing trend in the flexural strength although fluctuation occurs at mixes GNPs-030 and GNPs-070. The GNP-100 has the highest tensile strength of 8.62 MPa, increasing by around 20% compared with the control mix. It tends to confirm that the addition of GNPs has a beneficial influence on the flexural strength development as it can effectively blunt (diversion) and bridge the cracks (Rehman et al., 2018; Baomin and Shuang, 2019). This has been confirmed by a micro-graphical study (Farooq et al., 2020).

## Piezoresistive Properties

### Influence of Pre-drying Condition

**Figure 8** shows the influence of the drying condition on the mean electrical resistance change rate. It can be seen that without drying treatment, the resistance change rate is around 0.06% for all the mixes, which can be hardly detected in practice. Although the change rate is increased to around 0.5% after drying at 40°C for 14 days, this value is too small for structural health monitoring application. When a drying temperature of 105°C was applied for 1 day, a significant change rate is observed. The change rate is above 2% for a dosage of 0.1, 0.3, and 1.0 wt%, indicating a potential to be used for structural health monitoring. Furthermore, it should be noted that a significant drop of resistance change rate is observed for a GNPs dosage of 0.5

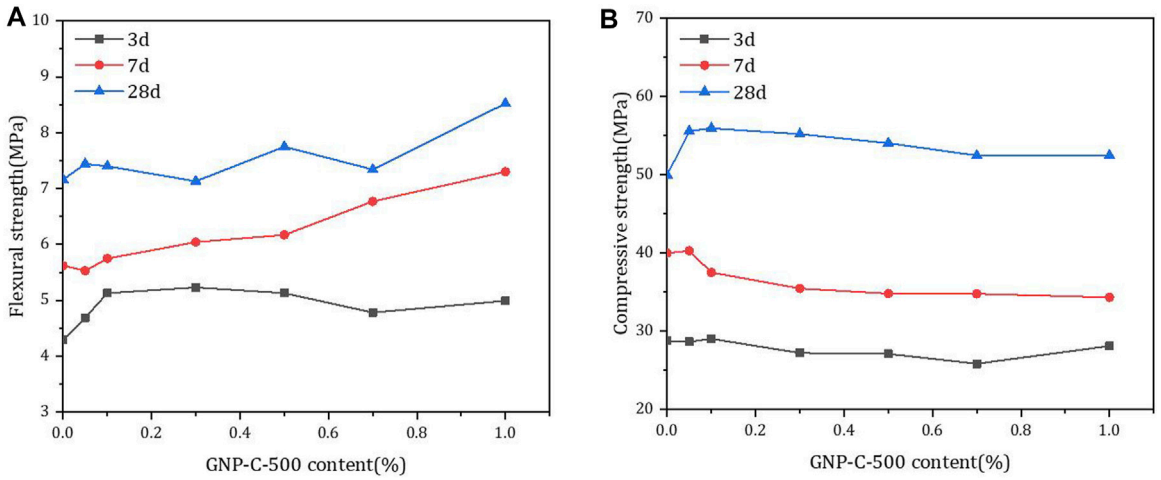


**FIGURE 7 |** The effects of curing age and the GNP-C-500 content on **(A)** flexural strength and **(B)** compress strength.

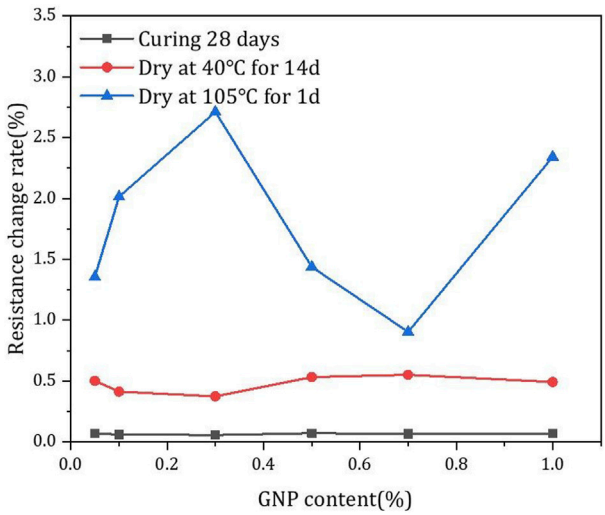


**FIGURE 8 |** The effects of drying conditions and the GNP-C-500 content on resistance change rate.

and 0.7 wt%. A possible reason could be the following. When the content of GNPs is low, the nano-particles stay far away from each other. Therefore, limited conductive links are generated and the electrical resistance of specimens is low. If the content of GNPs increases, many nano-particles are located within a certain percolation threshold to form conductive links. The connection of these links turns the samples to act as semi-conducts. The connections of these links are sensitive to the deformation of the loaded specimens. Therefore, the resistance change rate becomes high. If the content of GNPs is high, the nano-particles may be totally connected with each other by contact (Liu et al., 2016). Therefore, the influence of deformation of the specimens becomes weak on the resistance. However, when the GNPs dosage reaches 1.0 wt%, the agglomeration of GNPs become severe. A large number of isolated agglomeration of GNPs enables the resistance to be sensitive to the specimen deformation again. The GNPs-100 specimen dried under 105°C for 1 day was used for the piezoresistive properties measurements under cyclical loading. Mix GNPs-100 was used for the following studies.

## Influence of Loading Scheme

The measurement of average resistance change rate of GNPs-100 specimen at each load level under two loading schemes are shown in **Figure 9**. From **Figure 9A**, it can be seen that the average resistance change rate grows with amplitude. At the low stress amplitude, the resistance change rate increases faster than the high stress level. For example, the resistance change rate increases by 2% from when the amplitude grows from 4 to 8 MPa, while an increment of 0.7% is observed when 32 MPa amplitude is used compared with 28 MPa amplitude.

**Figure 9B** shows the average resistance change rate of each load cycle under pre-loaded conditions. Clearly, with the same amplitude, the growth of pre-loaded level causes a reduction of resistance change rate. Specifically, the average resistance change rate decreases from 2.7 to 0.72 when the pre-loaded stress level grows from 0.4 to 28 MPa.

## Influence of Microcracks

The average resistance change rate of the GNPs-100 specimens with microcracks are shown in **Figure 10** for the two loading conditions. Overall, the trend of resistance change rate has a significant change after cracking. In **Figure 10A**, there is a small increase at the low amplitude (<16 MPa) as the microcracks are closed by the loading. This is followed by a decline which can be attributed to the stable crack development. For the sustained cyclical load condition, see **Figure 10B**. The average resistance change rate is similar to the free cyclic loading condition. However, there is a significant increase above 28 MPa.

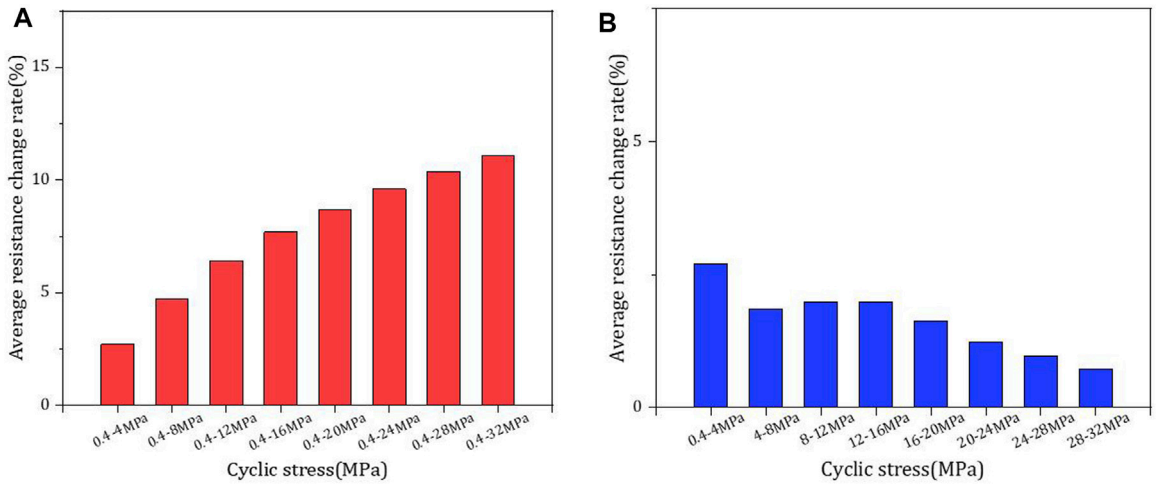


**FIGURE 9 |** The average resistance change rate: **(A)** under cyclic loading for different amplitudes; **(B)** under sustained cyclic loading.

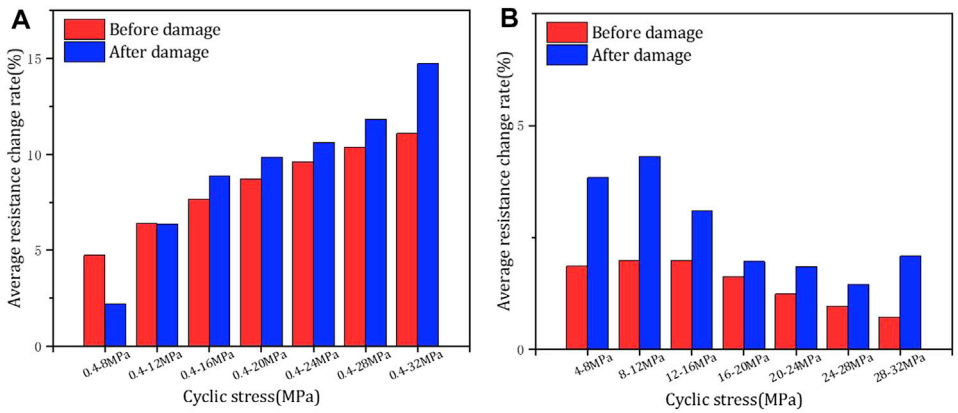


**FIGURE 10 |** Comparison of average resistance change rates: **(A)**under free cyclic loading at different stress levels before and after damage; **(B)**under load cyclic loading at different stress levels before and after damage.

### Resistance Change Rate-Time Diagram of Cyclic Loading

**Figure 11** shows the influence of the amplitude level on the resistance change rate-time diagram of GNPs-100. It can be seen that, with a small amplitude level, the diagram under each loading time follows a "V" shape, in which a sharp peak is observed when shifting from loading to unloading. With the amplitude growth, the strong linear relationship between resistance change rate and time gradually disappear. The "V" shape turns into a "U" shape diagram once the amplitude exceeds 20 MPa. From the application point of view, this feature has the potential to be used to distinguish the status of the specimens for the concrete structural health monitoring.

**Figure 12** shows the resistance change rate-time diagram of cracked GNPs-100 specimens under different sustained levels. It is clear that under sustained loading, the evolution of resistance change rate keeps the sharp peak, like "V", for all the loading levels. The resistance change rate and applied stress maintains a linear relationship. It means that even under a high stress sustained loading condition, the resistance change rate can be easily distinguished for the practical applications. This loading condition is more relevant to the status of structures in service.

## CONCLUSION

This work investigated the fresh properties, strength properties, and piezoresistive properties of the prepared GNPs-cement composites. Based on the results and analysis, the following conclusions were drawn:

The addition of GNPs has a negative effect on the workability and delays the setting time of the GNPs-cement composites. However, this does not hold for the dosage of 0.05 wt% in which the hydration seems to be facilitated by the GNPs.

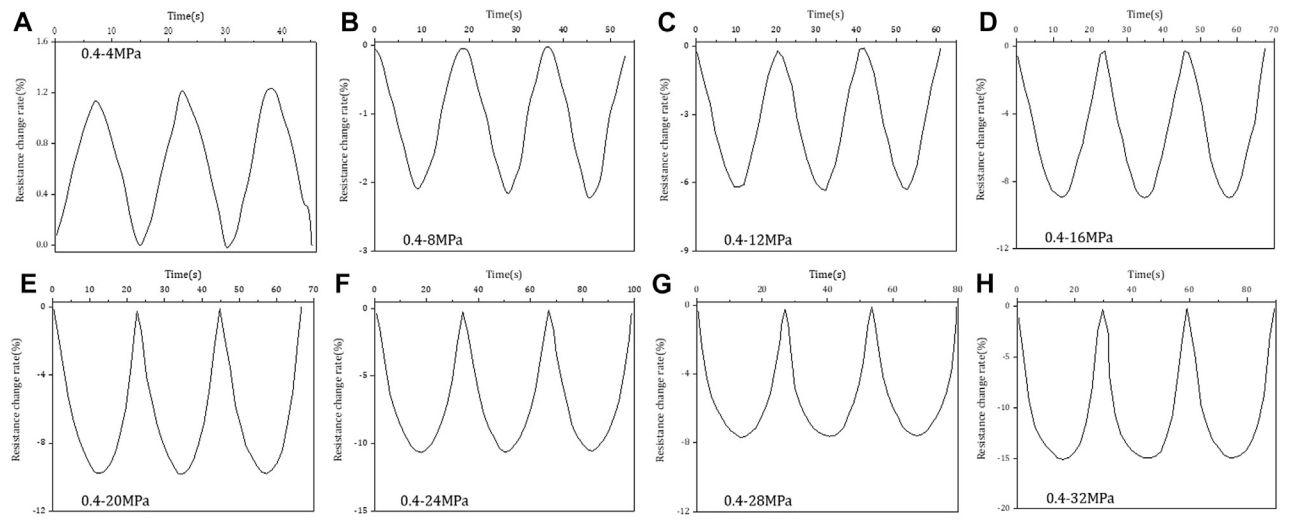


**FIGURE 11 |** Resistance change rate-time diagram of free cyclic loading. **(A)** Cyclic stess: 0.4–4 MPa; **(B)** Cyclic stess: 0.4–8 MPa; **(C)** Cyclic stess: 0.4–12 MPa; **(D)** Cyclic stess: 0.4–16 MPa; **(E)** Cyclic stess: 0.4–20 MPa; **(F)** Cyclic stess: 0.4–24 MPa; **(G)** Cyclic stess: 0.4–28 MPa; **(H)** Cyclic stess: 0.4–32 MPa.

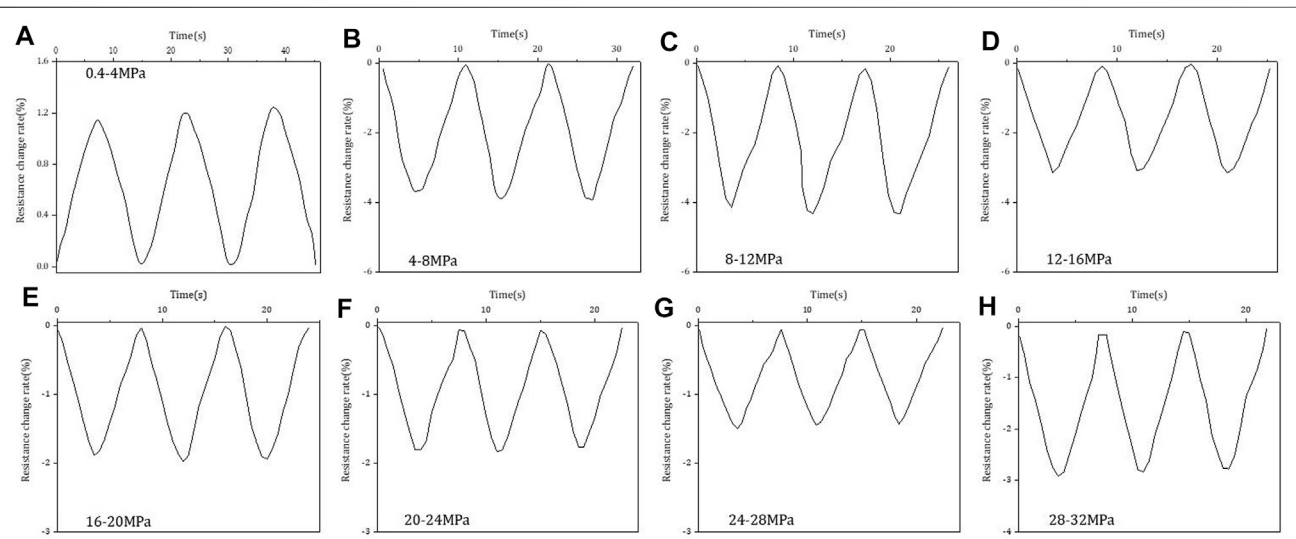


**FIGURE 12 |** Resistance change rate-time diagram of sustained cyclic loading condition: **(A)** Cyclic stess: 0.4–4 MPa; **(B)** Cyclic stess: 4–8 MPa; **(C)** Cyclic stess: 8–12 MPa; **(D)** Cyclic stess: 12–16 MPa; **(E)** Cyclic stess: 16–20 MPa; **(F)** Cyclic stess: 20–24 MPa; **(G)** Cyclic stess: 24–28 MPa; **(H)** Cyclic stess: 28–32 MPa.

The flowability of the fresh GNPs-mortar decreases with the GNPs increasing. When a GNP dosage of 1 wt% is used, the spread diameter decreases to 140 mm, 25% lower than the control mix.

The addition of GNPs shows different influence on the flexural and compressive loading resistance of the GNPs-mortar. In general, the flexural strength increases with the GNPs dosage for all the tests ages. The trend is more complex in terms of the compressive strength. At 3 and 7 days, the compressive strength of the GNPs-mortar specimens is lower than the control mix. However, this is not true for a small addition of GNPs (0.05 wt% of binder), which seems to promote the development of the compressive strength. After 7 days, there is a remarkable increment in compressive strength of the GNPs-mortar. At 28 days, the compressive of the GNPs-mortars becomes higher than the reference mortar specimen.

The pre-drying condition has a significant influence on the piezoresistive properties of the GNPs-mortar. It is shown that drying specimens under 105°C for 1 day can be regarded as a proper pre-treatment approach for improving the piezoresistive properties of GNPs-mortar.

After the proper drying treatment, the average resistance change rate can be above 2% for GNPs-010, GNPs-030, and GNPs-100 mixes.

The piezoresistive properties were conducted on the GNPs-100 mix under two different cyclical loading schemes. It has been shown that the average resistance change rate increases with the amplitude increasing and a reduction is observed for the sustained cyclical loading condition in terms of a pre-cracked specimens.

For the pre-cracked specimens (with microcracks), the evolution of the average resistance change has a remarkable change due to the crack propagation.

The resistance change rate-time diagram turns from a "V" to a "U"-like shape with the amplitude increase. This feature can be further used to distinguish the status of the specimen. On the other hand, in terms of the cracked specimens under sustained cyclical loading, the strong linear relationship remains for all the load levels.

Considering the flowability and mechanical and piezoresistive properties, GNPs-100 mix has the potential to be used for concrete structural health monitoring. Nevertheless, prior to its application, studies on performance under complex load conditions and properties related with durability are required.

## DATA AVAILABILITY STATEMENT

The raw data supporting the conclusion of this article will be made available by the authors, without undue reservation.

## AUTHOR CONTRIBUTIONS

ZG, JQ, RS, YG, HZ, and ZW performed the analyses and wrote the paper.

## FUNDING

ZG would like to acknowledge the funding offered by the National Natural Science Foundation of China (51478252, 51978387), Natural Science Foundation of Shandong Province (ZR2013EEM025, ZR2020QE271), and Key Technology Research and Development Program of Shandong (2015GSF122009). HZ would like to acknowledge the National Natural Science Foundation of China under grant 52008234, Taishan Scholars Foundation of Shandong Province under grant number tsqn201909032, and Natural Science Foundation of Jiangsu Province under grant number BK20200235.

## ACKNOWLEDGMENTS

Sincere gratitude is given to the research laboratory in the School of Qilu Transportation, Shandong University.

## SUPPLEMENTARY MATERIAL

The Supplementary Material for this article can be found online at: https://www.frontiersin.org/articles/10.3389/fbuil.2021.673346/full#supplementary-material

## REFERENCES

Alkhateb, H., Al-Ostaz, A., Cheng, A. H.-D., and Li, X. (2013). Materials Genome for Graphene-Cement Nanocomposites. *J. Nanomech. Micromech.* 3 (3), 67–77. doi:10.1061/(asce)nm.2153-5477.0000055

Baomin, W., and Shuang, D. (2019). Effect and Mechanism of Graphene Nanoplatelets on Hydration Reaction, Mechanical Properties and Microstructure of Cement Composites. *Constr. Build. Mater.* 228, 116720. doi:10.1016/j.conbuildmat.2019.116720

Birenboim, M., Nadiv, R., Alatawna, A., Buzaglo, M., Schahar, G., Lee, J., et al. (2019). Reinforcement and Workability Aspects of Graphene-Oxide-Reinforced Cement Nanocomposites. *Compos. B. Eng.* 161, 68–76. doi:10.1016/j.compositesb.2018.10.030

Chen, G., Yang, M., Xu, L., Zhang, Y., and Wang, Y. (2019). Graphene Nanoplatelets Impact on Concrete in Improving Freeze-Thaw Resistance. *Appl. Sci.* 9 (17), 3582. doi:10.3390/app9173582

Chen, P.-W., and Chung, D. D. L. (1996). Concrete as a New Strain/stress Sensor. *Compos. B. Eng.* 27 (1), 11–23. doi:10.1016/1359-8368(95)00002-x

Chu, K., Li, W.-s., and Dong, H. (2013). Role of Graphene Waviness on the thermal Conductivity of Graphene Composites. *Appl. Phys. A.* 111 (1), 221–225. doi:10.1007/s00339-012-7497-y

Dong, W., Li, W., Tao, Z., and Wang, K. (2019). Piezoresistive Properties of Cement-Based Sensors: Review and Perspective. *Constr. Build. Mater.* 203, 146–163. doi:10.1016/j.conbuildmat.2019.01.081

Du, H., and Pang, S. D. (2018). Dispersion and Stability of Graphene Nanoplatelet in Water and its Influence on Cement Composites. *Constr. Build. Mater.* 167, 403–413. doi:10.1016/j.conbuildmat.2018.02.046

Du, H., and Pang, S. D. (2015). Enhancement of Barrier Properties of Cement Mortar with Graphene Nanoplatelet. *Cement Concrete Res.* 76, 10–19. doi:10.1016/j.cemconres.2015.05.007

Du, M., Jing, H., Gao, Y., Su, H., and Fang, H. (2020). Carbon Nanomaterials Enhanced Cement-Based Composites: Advances and Challenges %. *Nanotechnol. Rev.* 9 (1), 115–135. doi:10.1515/ntrev-2020-0011

Farooq, F., Akbar, A., Khushnood, R. A., Muhammad, W. L. B., Rehman, S. K. U., and Javed, M. F. (2020). Experimental Investigation of Hybrid Carbon Nanotubes and Graphite Nanoplatelets on Rheology, Shrinkage, Mechanical, and Microstructure of SCCM. *Materials* 13 (1), 230. doi:10.3390/ma13010230

Gholampour, A., Valizadeh Kiamahalleh, M., Tran, D. N. H., Ozbakkaloglu, T., and Losic, D. (2017). From Graphene Oxide to Reduced Graphene Oxide: Impact on the Physiochemical and Mechanical Properties of Graphene-Cement Composites. *ACS Appl. Mater. Inter.* 9 (49), 43275–43286. doi:10.1021/acsami.7b16736

Guo, L., Wu, J., and Wang, H. (2020). Mechanical and Perceptual Characterization of Ultra-high-performance Cement-Based Composites with Silane-Treated Graphene Nano-Platelets. *Constr. Build. Mater.* 240, 117926. doi:10.1016/j.conbuildmat.2019.117926

Han, B., and Ou, J. (2007). Embedded Piezoresistive Cement-Based Stress/strain Sensor. *Sensors Actuators A. Phys.* 138 (2), 294–298. doi:10.1016/j.sna.2007.05.011

Hou, D., Zhang, W., Ge, Z., Wang, P., Wang, X., and Zhang, H. (2021). Experimentally Validated Peridynamic Fracture Modelling of Mortar at the Meso-Scale. *Constr. Build. Mater.* 267. doi:10.1016/j.conbuildmat.2020.120939

Jaitanong, N., Narksitipan, S., Ngamjarurojana, A., and Chaipanich, A. (2018). Influence of Graphene Nanoplatelets on Morphological and Electrical Properties of Silica Fume Blended Cement - Piezoelectric Ceramic Composite. *Ceramics Int.* 44, S137–S140. doi:10.1016/j.ceramint.2018.08.131

Le, J.-L., Du, H., and Pang, S. D. (2014). Use of 2D Graphene Nanoplatelets (GNP) in Cement Composites for Structural Health Evaluation. *Compos. B. Eng.* 67, 555–563. doi:10.1016/j.compositesb.2014.08.005

Li, S., Cao, Y., Qi, J., Liu, H., and Moheimani, R. (2020). Developing a Nested Micromechanical Model to Predict the Relaxation Moduli of Graphene Nanoplatelets/carbon Fiber Reinforced Hybrid Nanocomposites. *Proc. Inst. Mech. Eng. L: J. Mater. Des. Appl.* 234 (3), 504–519. doi:10.1177/1464420719899971

Li, Z. J., Zhang, D., and Wu, K. R. (2001). Cement Matrix 2-2 Piezoelectric Composite-Part 1. Sensory Effect. *Mat. Struct.* 34 (8), 506–512. doi:10.1007/bf02486500

Lin, Y., and Du, H. (2020). Graphene Reinforced Cement Composites: A Review. *Constr. Build. Mater.* 265, 120312. doi:10.1016/j.conbuildmat.2020.120312

Liu, Q., Gao, R., Tam, V. W. Y., Li, W., and Xiao, J. (2018). Strain Monitoring for a Bending concrete Beam by Using Piezoresistive Cement-Based Sensors. *Constr. Build. Mater.* 167, 338–347. doi:10.1016/j.conbuildmat.2018.02.048

Liu, Q., Xu, Q., Yu, Q., Gao, R., and Tong, T. (2016). Experimental Investigation on Mechanical and Piezoresistive Properties of Cementitious Materials Containing Graphene and Graphene Oxide Nanoplatelets. *Constr. Build. Mater.* 127, 565–576. doi:10.1016/j.conbuildmat.2016.10.024

Luo, D., Ismail, Z., and Ibrahim, Z. (2013). Added Advantages in Using a Fiber Bragg Grating Sensor in the Determination of Early Age Setting Time for Cement Pastes. *Measurement* 46 (10), 4313–4320. doi:10.1016/j.measurement.2013.06.036

Peyvandi, A., Soroushian, P., Abdol, N., and Balachandra, A. M. (2013). Surface-modified Graphite Nanomaterials for Improved Reinforcement Efficiency in Cementitious Paste. *Carbon* 63, 175–186. doi:10.1016/j.carbon.2013.06.069

Pu, N.-W., Wang, C.-A., Liu, Y.-M., Sung, Y., Wang, D.-S., and Ger, M.-D. (2012). Dispersion of Graphene in Aqueous Solutions with Different Types of Surfactants and the Production of Graphene Films by spray or Drop Coating. *J. Taiwan Inst. Chem. Eng.* 43 (1), 140–146. doi:10.1016/j.jtice.2011.06.012

Qureshi, T. S., and Panesar, D. K. (2020). Nano Reinforced Cement Paste Composite with Functionalized Graphene and Pristine Graphene Nanoplatelets. *Compos. B. Eng.* 197. doi:10.1016/j.compositesb.2020.108063

Qureshi, T. S., and Panesar, D. K. (2019). Impact of Graphene Oxide and Highly Reduced Graphene Oxide on Cement Based Composites. *Constr. Build. Mater.* 206, 71–83. doi:10.1016/j.conbuildmat.2019.01.176

Qureshi, T. S., Panesar, D. K., Sidhureddy, B., Chen, A., and Wood, P. C. (2019). Nano-cement Composite with Graphene Oxide Produced from Epigenetic Graphite deposit. *Compos. B. Eng.* 159, 248–258. doi:10.1016/j.compositesb.2018.09.095

Rehman, S. K. U., Ibrahim, Z., Jameel, M., Memon, S. A., Javed, M. F., Aslam, M., et al. (2018). Assessment of Rheological and Piezoresistive Properties of Graphene Based Cement Composites. *Int. J. Concrete Structures Mater.* 12 (1), 64. doi:10.1186/s40069-018-0293-0

Shi, Z.-Q., and Chung, D. D. L. (1999). Carbon Fiber-Reinforced concrete for Traffic Monitoring and Weighing in Motion. *Cement Concrete Res.* 29 (3), 435–439. doi:10.1016/s0008-8846(98)00204-x

Sun, S., Ding, S., Han, B., Dong, S., Yu, X., Zhou, D., et al. (2017). Multi-layer Graphene-Engineered Cementitious Composites with Multifunctionality/intelligence. *Compos. B. Eng.* 129, 221–232. doi:10.1016/j.compositesb.2017.07.063

Tao, J., Wang, X., Wang, Z., and Zeng, Q. (2019). Graphene Nanoplatelets as an Effective Additive to Tune the Microstructures and Piezoresistive Properties of Cement-Based Composites. *Constr. Build. Mater.* 209, 665–678. doi:10.1016/j.conbuildmat.2019.03.173

Tong, T., Fan, Z., Liu, Q., Wang, S., Tan, S., and Yu, Q. (2016). Investigation of the Effects of Graphene and Graphene Oxide Nanoplatelets on the Micro- and Macro-Properties of Cementitious Materials. *Constr. Build. Mater.* 106, 102–114. doi:10.1016/j.conbuildmat.2015.12.092

Wang, B., Jiang, R., and Wu, Z. (2016). Investigation of the Mechanical Properties and Microstructure of Graphene Nanoplatelet-Cement Composite. *Nanomaterials* 6 (11), 200. doi:10.3390/nano6110200

Wang, B., and Pang, B. (2019). Mechanical Property and Toughening Mechanism of Water Reducing Agents Modified Graphene Nanoplatelets Reinforced Cement Composites. *Constr. Build. Mater.* 226, 699–711. doi:10.1016/j.conbuildmat.2019.07.229

Wang, B., and Shuang, D. (2018). Effect of Graphene Nanoplatelets on the Properties, Pore Structure and Microstructure of Cement Composites. *Mat. Express* 8 (5), 407–416. doi:10.1166/mex.2018.1447

Wei, W., Lu, W., and Yang, Q. H. (2011). High-concentration Graphene Aqueous Suspension and a Membrane Self-Assembled at the Liquid-Air Interface. *Xinxing Tan Cailiao/New Carbon Mater.* 26 (1), 36–40. doi:10.1016/J.CARBON.2011.02.037

Xu, J., and Zhang, D. (2017). Pressure-sensitive Properties of Emulsion Modified Graphene Nanoplatelets/cement Composites. *Cem. Concr. Comp.* 84, 74–82. doi:10.1016/j.cemconcomp.2017.07.025

Yoo, D.-Y., Kim, S., and Lee, S. H. (2018). Self-sensing Capability of Ultra-high-performance concrete Containing Steel Fibers and Carbon Nanotubes under Tension. *Sensors Actuators A. Phys.* 276, 125–136. doi:10.1016/j.sna.2018.04.009

Zhang, D., Li, Z., and Wu, K.-R. (2002). 2-2 Piezoelectric Cement Matrix Composite: Part II. Actuator Effect. *Cement Concrete Res.* 32 (5), 825–830. doi:10.1016/s0008-8846(01)00761-x

Zhang, H., Xu, Y., Gan, Y., Schlangen, E., and Šavija, B. (2020). Experimentally Validated Meso-Scale Fracture Modelling of Mortar Using Output from Micromechanical Models. *Cem. Concr. Compos.* 110, 1–12. doi:10.1016/j.cemconcomp.2020.103567

**Conflict of Interest:** Author ZW was employed by company Shandong Hi-Speed Group.

The remaining authors declare that the research was conducted in the absence of any commercial or financial relationships that could be construed as a potential conflict of interest.

**Publisher's Note:** All claims expressed in this article are solely those of the authors and do not necessarily represent those of their affiliated organizations, or those of the publisher, the editors and the reviewers. Any product that may be evaluated in this article, or claim that may be made by its manufacturer, is not guaranteed or endorsed by the publisher.